



ELSEVIER

Contents lists available at ScienceDirect

Electrochimica Acta

journal homepage: www.elsevier.com/locate/electacta

Nanomolar detection of mercury(II) using electropolymerized phthalocyanine film

Manjunatha Palanna, Shambhulinga Aralekallu, CP Keshavananda Prabhu, Veeresh A Sajjan, Mounesh, Lokesh Koodlur Sannegowda*

Department of Studies in Chemistry, Vijayanagara Sri Krishnadevaraya University, Ballari, 583105, Karnataka, India



ARTICLE INFO

Article history:

Received 21 August 2020

Revised 24 October 2020

Accepted 19 November 2020

Available online 25 November 2020

Keywords:

Benzimidazole phthalocyanine

Electropolymerization

Mercury(II)

Cyclic voltammetry

Chronoamperometry

ABSTRACT

The synthesis and characterization of novel cobalt(II) tetraamide benzimidazole phthalocyanine (CoTABImPc) has been reported for the first time and applied for the determination of mercury(II) at nanomolar concentration using electrochemical techniques. CoTABImPc was prepared by coupling 4-(1H-benzimidazol-2-yl)aniline with cobalt(II) tetracarboxylic acid phthalocyanine. CoTABImPc was characterized by elemental analysis, TGA, FT-IR, UV-visible, Mass, and NMR spectroscopic techniques. The CoTABImPc was electropolymerized on clean glassy carbon electrode (GCE) by continuous cycling of the potential (GCE/poly(CoTABImPc)). The polymeric film was employed for the detection of highly toxic Hg(II) by cyclic voltammetry (CV), differential pulse voltammetry (DPV) and chronoamperometric (CA) methods. The designed GCE/poly(CoTABImPc) electrode exhibited good electrochemical response and high electrocatalytic activity for detecting Hg(II). The Pc polymeric film electrode displayed a sensitivity of $1.2178 \mu\text{A nM}^{-1} \text{cm}^{-2}$ for the detection of Hg(II) in the linear range 10–300 nM, and low detection limit of 4 nM using CV technique. Further, DPV exhibited a sensitivity of $1.4024 \mu\text{A nM}^{-1} \text{cm}^{-2}$ in the 10–500 nM range with LOD of 3.8 nM. The CA method delivered an excellent sensitivity of $3.7389 \mu\text{A nM}^{-1} \text{cm}^{-2}$ in the linear range 10–400 nM with LOD of 3 nM. The proposed method augments the selective electrochemical determination of Hg(II) in environment pollution analysis.

© 2020 Elsevier Ltd. All rights reserved.

1. Introduction

Heavy metal ions like As, Cd, Pb, Cr and Hg are highly harmful to the environment and human health [1]. Heavy metal ions from industrial wastewater are majorly responsible for water pollution [2]. Heavy metal ions get enriched in the living organisms through the food chain and due to their nondegradability and non-biocompatibility results in serious damage and problems to animals, plants, and humans. Particularly, mercury (Hg(II)) is considered as the most toxic element that could easily accumulate in the human body and environment [3]. The World Health Organization (WHO) has set a permissible level of Hg(II) as 30 ppb in drinking water, whilst the U.S Food and Drug Administration corporation has mentioned a maximum permissible level of Hg(II) in meat as 1000 nM L^{-1} [4].

Among the different Hg compounds, most dangerous is dimethylmercury ($(\text{CH}_3)_2\text{Hg}$) which is toxic enough to cause death even if few microliters is spilt on the skin, or even on latex

gloves [5]. The excess Hg(II) levels in water and meat can lead to death, mental retardation, dysarthria, blindness, neurological deficits, hearing impairment, developmental defects, and abnormal muscle tone [6]. Besides, it can result in disorders including Hunter-Russell syndrome, pink disease, Minamata disease and severe kidney damage. Hence the contamination caused by heavy metals has aroused extensive public concern [4].

In this regard, accurate, reliable detection, and monitoring of trace level Hg(II) in water, as well as noxious waste samples, has profound importance to secure the health and environment. Different analytical methods have been developed for the reliable detection of Hg(II), including traditional methods such as inductively coupled atomic absorption and emission spectroscopy [7], X-ray fluorescence spectrometry [8], inductively coupled plasma mass spectrometry [9] and capillary electrophoresis [10]. Also, different sensing strategies have been explored for the detection of Hg(II) using photoelectrochemical [11], surface Plasmon resonance [12], surface-enhanced resonance Raman scattering [13], electrochemical [14], fluorescence and colorimetric methods [15, 16].

However, among the various analytical methods, electrochemical methods are simple, reliable and straightforward when compared with the accessible aforementioned conventional and ad-

* Corresponding author.

E-mail address: kslokesh@vskub.ac.in (L.K. Sannegowda).

vanced methods. But the electrochemical techniques require an appropriate catalyst which can reduce the overpotential and increase the catalytic activity.

In recent years, metal phthalocyanines (Pcs) have clinched great interest because of their excellent properties like environment-friendliness, low-cost, stability, and semiconducting nature [17]. Moreover, Pcs are easy to synthesize and are widely studied as sensors [18–20], supercapacitors and battery [21, 22] materials in succession to their traditional applications as dyes and pigments [23]. Metal phthalocyanines (MPcs) are redox-active molecules and are known to catalyze the reactions effectively [24–27].

Hence, MPcs find great potential as surface modifiers in electrochemical sensors as they yield high surface area, good absorbability, and high catalytic activity [28]. A variety of MPcs composed of different metal ions and ligands have been reported as efficient catalysts in electrochemical sensors [29, 30]. Among them, Co-based MPcs are explored extensively, as they exhibit exceptional chemical stability and flexibility for catalytic applications [31, 32]. However Pc-based materials have not yet been employed in the electrochemical sensing of heavy metals and in particular Hg(II).

The benzimidazole substituent at the periphery of Pc ring is electrochemically active and it forms an electropolymerized film on potential cycling [33]. The polymeric film deposits on the electrode surface and provides chemical interaction between the electrode and Pc polymeric film. The Pc film uniformly distributes and expected to have high conductivity due to the extension of conjugation and delocalization with higher surface area and also, provides higher stability and less interfacial resistance for the charge transfer compared to physical adsorption process [34].

In this study, CoTABImPc was prepared for the first time and was electropolymerized and utilized as a highly sensitive and selective catalyst for Hg(II) electrochemical sensor.

2. Experimental section

2.1. Materials

4-aminobenzoic acid, anhydrous cobaltous acetate, anhydrous potassium carbonate, orthophenylenediamine and mercury(II) chloride were procured from Alfa Aesar India. 5% Nafion solution, N, N'-dicyclohexylcarbodiimide, dimethylsulphoxide, N, N'-dimethylformamide, methanol, ethanol were purchased from Merck, India. Electrodes were obtained from fuel cell store, India.

2.2. Synthesis of phthalocyanine complex

2.2.1. Synthesis of cobalt(II) tetraamide benzimidazole phthalocyanine complex

The synthesis of CoTABImPc was performed as revealed in Scheme 1. The preparation of benzimidazole phthalocyanine complex has two reaction steps. The first step involves the formation of 4-aminobenzimidazole moiety and the second step is the coupling of the precursor with carboxylic acid phthalocyanine to yield the cobalt tetraamide benzimidazole phthalocyanine complex as the concluding product.

2.2.2. Preparation of 4-(1H-benzimidazol-2-yl)aniline (i)

The mixture of o-phenylenediamine (2.531 g, 0.0234 mol) and 4-aminobenzoic acid (3.209 g, 0.0234 mol) was grounded well and transferred into a clean dried RB flask containing ethanol (20 mL) as a solvent and added a catalytic amount of NH₄Cl to the solution and refluxed at 65–70 °C for 4 h to get compound i. The reaction progress was monitored using thin-layer chromatography (TLC). After completion of the product formation, crude was charged into deionized ice-cold water to get a brown precipitate. The product obtained was filtered, washed with distilled water and finally, the

crude product was purified using chloroform to get corresponding 4-(1H-benzimidazol-2-yl)aniline [35].

Yield: 73%. Melting point: 226–228 °C. Anal. for (i), Mol. Wt. 209.26. C₁₃H₁₁N₃; Calc. (%): C, 74.62; H, 5.30; N, 20.08. Found (%): C, 74.43; H, 5.33; N, 20.32. IR absorption bands (KBr (pellet), cm⁻¹): 494, 691, 730, 897, 922, 1001, 1031, 1109, 1243, 1273, 1312, 1460, 1479, 1568, 1666, 1760, 1878, 1918, 2763, 3057, 3216, 3343 and 3432. ¹H NMR (400 MHz, DMSO-d₆): δ 5.58 (s, 2H), 7.47 (d, J = 8.00 Hz, 1H), 7.56 (d, J = 9.00 Hz, 1H), 7.88 (d, J = 9.00 Hz, 1H), 7.49 (d, J = 8 Hz, 1H), 11.38 (s, 1H). Mass: M⁺(212.13).

2.2.3. Preparation of cobalt(II) tetracarboxylic acid phthalocyanine complex (CoTCAPc) (ii)

CoTCAPc was synthesized by utilizing the procedure as reported in the literature [33, 34]. A ground mixture of trimellitic anhydride (100 mM), urea (5 M), a catalytic amount of ammonium molybdate (0.2 mM) and CoCl₂ (25 mM) was charged into a three-necked flask and stirred at 170–180 °C for 5 h and then cooled to room temperature. The obtained shady green colored product was purified by washing with alcohol and concurrently with hot dil.HCl and 1 N NaOH solutions. At last, CoTCAPc was washed with a large amount of distilled water to remove the acid. The product CoTCAPc was dried over P₂O₅.

Yield: 78%. Anal. CoTCAPc, Mol. Wt. 747.49. C₃₆H₁₆N₈O₈Co; Calc. (%): C, 57.84; H, 2.16; N, 14.99; O, 17.12; Co, 7.88. Found: C, 57.52; H, 2.13; N, 15.24; Co, 7.75. Absorption spectra (DMSO, λ_{max}(nm)): 330, 430, 600, 635. IR absorption bands (KBr (pellet), cm⁻¹): 736, 884, 1091, 1157, 1283, 1323, 1403, 1469, 1520, 1606, 1718, 2224, 2851, 2927, and 3406. Mass: M⁺(747).

2.2.4. Synthesis of cobalt(II) tetraamide benzimidazole phthalocyanine complex (iii)

The precursor compound 4-(1H-benzimidazol-2-yl)aniline (1.01 g, 0.0040 mol) was mixed with CoTCAPc (0.241 g, 0.0010 mol) and, DCC (1.51 g, 0.0060 mol) in an RB flask containing 10 mL dimethylformamide. The mixture was refluxed at 90 °C for about 6 h. The dim bluish-green colored product formed was washed with alcohol, hexane and acetone. Then dried in an oven at 60 °C for an overnight.

Yield: 75%. Anal. for CoTABImPc (deep blue), Mol. Wt. 1512.42 C₈₈H₅₂N₂₀O₄Co; Calc. (%): C, 69.88; H, 3.47; N, 18.52; Co, 3.90; O, 4.23. Found (%): C, 69.49; H, 3.41; N, 18.79; Co, 3.61. Absorption spectra (DMSO, λ_{max}/ nm (log ε, mol⁻¹ L cm⁻¹)): 339 (3.69), 612 (4.03), 677 (4.21). IR absorption bands (KBr (pellet), cm⁻¹): 642, 722, 752, 806, 892, 1043, 1090, 1154, 1244, 1309, 1446, 1578, 1625, 2123, 2856, 2930, 3217, 3349, and 3430. Mass: M⁺(1509.18).

2.3. Instrumentation and characterization

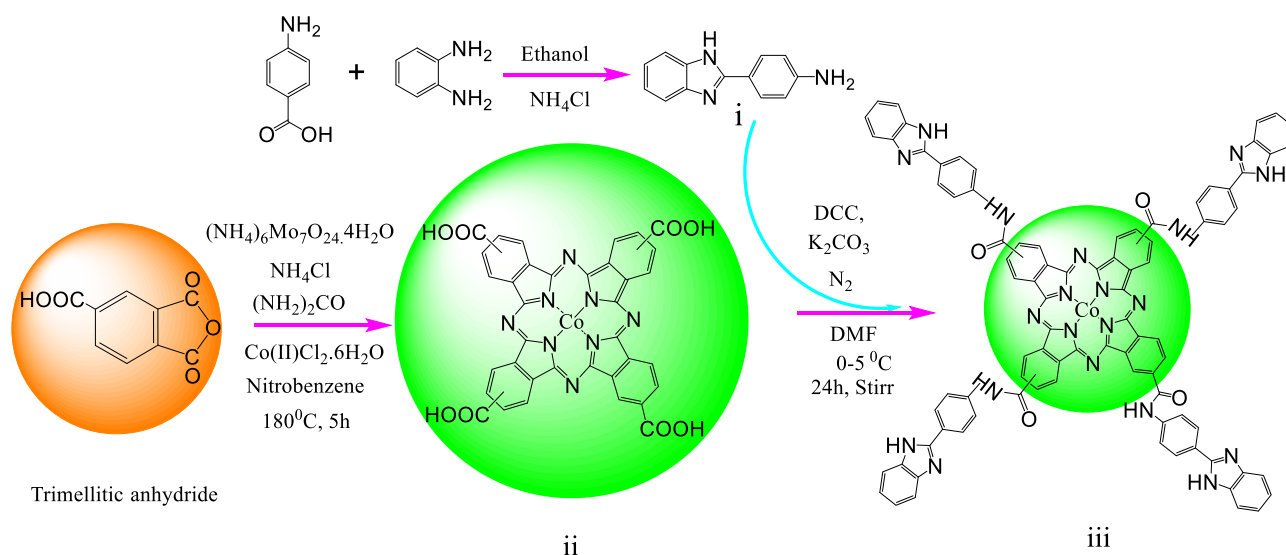
All the analytical techniques used for the characterization are mentioned in the Supporting Information.

2.4. Cleaning of glassy carbon electrode (GCE)

The GCE surface was polished with alumina powder slurry (0.3 and 0.05 μm, respectively) on a polishing pad. The polished electrode was then sonicated in ethanol to remove the trapped particles. Then CV scans were performed in –1 to 1 V range in 1 M H₂SO₄ electrolyte to remove the adsorbed particles on the surface of the GCE.

2.5. Modification of the electrode

The electropolymerization methodology was employed to deposit a thin uniform film of Pc on the electrode. Electropolymerization process was carried out using cyclic voltammetry with 0.1 mM



Scheme 1. Synthetic approach for CoTABImPc.

CoTABImPc in DMSO containing 0.1 M TBAP at cleaned GCE. The polymeric film electrode was represented as GCE/poly(CoTABImPc) and employed for voltammetric and amperometric determination of Hg(II).

2.6. Preparation of mercury(II) solution

The 0.01 M mercury(II) chloride stock solution was prepared using doubly distilled water and was diluted to achieve a working standard solution of 0.01 mM. Different aliquots of the standard solution of Hg(II) was injected into 10 mL PBS electrolyte throughout the analysis.

3. Results and discussion

The scheme for preparing cobalt tetraamide benzimidazole phthalocyanine (CoTABImPc) is presented in Scheme 1. The precursor **i** was prepared by reacting 4-aminobenzoic acid with OPDA in the presence of ethanol with a catalytic amount of NH_4Cl . The CoTABImPc formation involves the coupling of 4-aminobenzimidazole with CoTCAPc (Scheme 1).

The amide bond formation mechanism is presented in the Supporting Information (Scheme. S1). The amide bond is formed by the reaction of an acid and amine in the presence of a coupling agent. The amide bond is stable because of the resonance structure of $(-\text{CO}=\text{NH}-)$. The nitrogen in amide is having lone pair of electron capable of delocalization with carbonyl carbon. This forms the partial double bond between $-\text{N}=\text{C}$ by pushing electrons from $\text{C}=\text{O}$ and results, in turn, the formation of oxygen anion [36].

The electrophilic carbonyl carbon ($-\text{COOH}$) of CoTCAPc reacts with a nucleophilic amine group ($-\text{NH}_2$) of 4-amino benzimidazole in the presence of coupling agent dicyclohexylcarbodiimide (DCC) resulting in protonation/deprotonation. DCC acts as a dehydrating agent and also enhances the synthetic efficiency of the forward reaction forming the product. This coupling method is mild, efficient and compatible for peptide bond formation and the driving force of the reaction is the formation of urea by-product. The CoTABImPc complex obtained was bluish-green amorphous powder. The complex is soluble in DMF, DMSO, DMA, quinoline and Conc H_2SO_4 .

3.1. FT-IR studies

Fig. 1 depicts the FTIR spectra of precursor compound 4-aminobenzimidazole, CoTCAPc, and CoTABImPc complexes

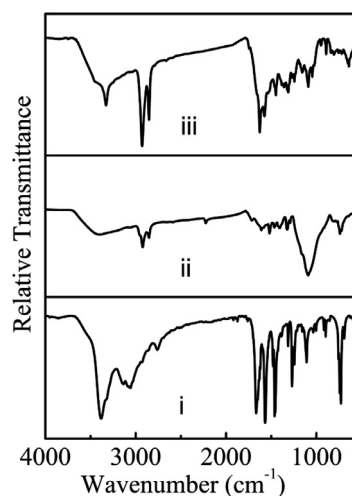


Fig. 1. FTIR spectra for (i) 4-(1H-benzimidazol-2-yl)aniline, (ii) CoTCAPc and (iii) CoTABImPc.

recorded in the range of 400–4000 cm^{-1} . The compound 4-aminobenzimidazole displayed peaks at 3343, 3216 and 3432 cm^{-1} corresponding to $-\text{NH}_2$ and $-\text{NH}$ of benzimidazole group. The characteristic peaks for Pc complex were observed around 735–750, 875–890, 1050–1060, 1090, 1150–1160 cm^{-1} and assigned for phthalocyanine skeletal vibrations [34]. The peak at 1718 cm^{-1} in the spectrum of CoTCAPc corresponds to $-\text{C}=\text{O}$ and broad peak at 3406 cm^{-1} for $-\text{OH}$ of $-\text{COOH}$ present in the complex. The disappearance of peaks at 3406 cm^{-1} and the appearance of a new peak at 3217 and 3349 cm^{-1} indicate the conversion of carboxylic acid Pc to benzimidazole cobalt phthalocyanine. The peak at 3430 cm^{-1} can be assigned for $-\text{NH}$ of benzimidazole group.

3.2. Mass spectra

The mass spectra of CoTCAPc and CoTABImPc are characterized by many competitive and consecutive pathways, thus forming many intense fragment ions. The mass spectrum was recorded at various retention times and the mass spectrum of the precursor compound 4-(1H-benzimidazol-2-yl)aniline is in Fig. S1. The

base peak for **i** appears at $m/z = 212.13$ which corresponds to M^{+3} molecular ion peak. The theoretical molecular weight of CoTCAPc is 747.49 and the mass spectrum demonstrated peaks at $m/z = 743, 744, 745, 746$ and 747.0 which can be accounted for $M^{-4}, M^{-3}, M^{-2}, M^{-1}$ and $M\cdot$ molecular ion peaks, Fig. S2. Similarly, CoTABImPc has a theoretical molecular mass of 1512.4 and the peak appeared at $m/z = 1509, 1527, 1528, 1529$ and 1530 can be attributed to $M^{-3}, (M+H_2O)^{-3}, (M+H_2O)^{-2}, (M+H_2O)^{-1}, (M+H_2O)$ molecular ion peaks as shown in Fig. S3.

3.3. $^1\text{H NMR}$ studies

The ^1H NMR spectrum of the precursor was measured in DMSO- d_6 at 400 MHz and chemical shift values were recorded in ppm. Fig. S4 is the ^1H NMR spectrum of 4-aminobenzimidazole and the peaks were observed at δ 5.58 (s, 2H), 7.47 (d, $J = 8.00$ Hz, 1H), 7.56 (d, $J = 9.00$ Hz, 1H), 7.88 (d, $J = 9.00$ Hz, 1H), 7.49 (d, $J = 8$ Hz, 1H), 11.38 (s, 1H). The peak for NH_2 of amine (in Fig. S4) was singlet peak at δ 5.58 (s, 2H) and peak for NH proton appeared at δ 11.38 (s, 1H). ^1H NMR spectrum successfully confirmed the purity and formation of 4-aminobenzimidazole compound (**i**).

3.4. UV-visible studies

Two characteristic bands were noticed in the UV-vis spectrum of phthalocyanine complexes i.e., B band or solet band in the UV region and Q band in the visible region (Fig. S5). The spectrum of CoTCAPc exhibited a peak at 330 nm in B band region and 635 nm in the Q band region with a shoulder peak at 600 nm. Whereas, CoTABImPc displayed a peak at 339 and 677 nm in B and Q band regions with a shoulder peak at 612 nm. The shoulder peak can be ascribed to vibronic nature as well as a dimer, oligomeric molecules present in the complex. The Q-band is responsible for the green color of the Pc complexes prepared. The small shift in the absorption peak position towards longer wavelength for CoTABImPc compared to CoTCAPc can be accounted for augmenting in the conjugation and resonance stabilization in benzimidazole phthalocyanine.

3.5. TGA studies

Fig. S6 depicts the thermograms of CoTCAPc and CoTABImPc. The little weight loss below 150 °C can be accounted to the loss of moisture and volatile components in the sample. The complexes were stable up to 450 °C and then the Pc macrocycle undergoes gradual decomposition in 400–550 °C region. At this temperature, the peripheral functional groups first get detached and then the complex undergoes decomposition in air atmosphere. The weight corresponding to the horizontal portion after 600 °C represents the stable oxidized compound, CoO formed which is equivalent to the theoretical weight of the CoO in the initial weight of Pc. The CoTABImPc demonstrated enhanced thermal stability than the CoTCAPc as a result of higher conjugation and extended delocalization in the CoTABImPc.

3.6. Cyclic voltammetric studies

The electrochemical activity and redox performance of the CoTABImPc complex was investigated by cyclic voltammetry (CV). Before the experiments, the DMSO solution was purged with a constant flow of N_2 gas to eliminate the dissolved oxygen for 20 min. Fig. 2 shows the first cyclic voltammogram for 1 mM CoTABImPc in DMSO containing 0.1 M TBAP as supporting electrolyte at a scan rate of 50 mVs^{-1} on pristine GCE. The CV of CoTABImPc demonstrated two pairs of redox peaks at -0.3 to -0.5 V and 0.25 to 0.45 V which can be assigned for the

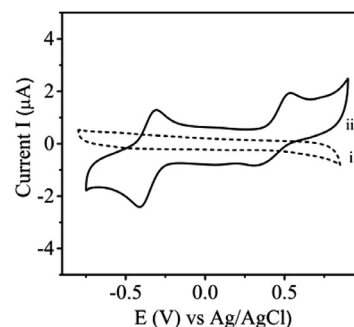


Fig. 2. CVs for (i) blank and (ii) 1 mM CoTABImPc in DMSO containing 0.1 M TBAP on GCE at 50 mVs^{-1} in N_2 atmosphere.

$[\text{Co}^{\text{II}}\text{Pc}^{-2}]/[\text{Co}^{\text{I}}\text{Pc}^{-1}]$ and $[\text{Co}^{\text{II}}\text{Pc}^{-2}]/[\text{Co}^{\text{I}}\text{Pc}^{-2}]$ redox couples, respectively according to the literature reports [29–31].

3.7. Electrochemical polymerization of CoTABImPc

The benzimidazole moiety is electrochemically active and it successfully forms polymerization product on continuous cycling of the potential. The electropolymerization of CoTABImPc was carried out on cleaned GCE with 0.1 M CoTABImPc in DMSO containing TBAP supporting electrolyte and scanning the potential amid 1 to -1 V at 20 mV s^{-1} for 20 cycles under the N_2 atmosphere as presented in Fig. S7. The gradual progress in the number of potential cycles displayed a proportional change in the current which is accounted for the sequential addition of repeating units to the polymer on the electrode. Further, peak potential shift was noticed for the consecutive CVs which might be due to the exposure of new polymeric surface at the GCE. The dark sapphire film was noticed after the deposition of polymer on the GCE surface. Polymerization of CoTABImPc complex involves the stacking of the supramolecular blocks with great structural flexibility. It is noteworthy that the acidity of the $-\text{NH}$ proton of benzimidazole moiety increases in presence of electronegative atoms located near the carbon atom. The interactions between electron-withdrawing and donating atoms are believed to be electrostatic interactions between π -donors and π -acceptors, which have been efficiently utilized in electrochemical polymerization [33, 34].

The polymeric film was analysed by CV to evaluate its electrochemical behavior and stability in DMSO containing 0.1 M TBAP at 20 mVs^{-1} under N_2 atmosphere. The first cycle in Fig S7, displayed peaks analogous to peaks in Fig. 2 which confirmed the adhering of poly(CoTABImPc) film on the electrode surface. Besides, Fig. S8 depicts a small or negligible change in the background and peak current for the fresh CV and the 100th cycle which infers that the poly(CoTABImPc) possess good electrochemical stability on the electrode.

3.8. Charge transfer behavior

Redox probe, Ferro/ferricyanide system was employed to evaluate the electron transfer characteristics of GCE/poly(CoTABImPc). Fig. S9 depicts the CVs of the redox probe at virgin GCE and GCE/poly(CoTABImPc) film. The virgin GCE showed well-defined characteristic redox peaks for the $\text{Fe}^{2+}/\text{Fe}^{3+}$ redox probe whereas, partial flattening of the peaks was noticed at the GCE/poly(CoTABImPc) with a peak current decrease which infers that the electron transfer is sluggish at the GCE/poly(CoTABImPc) compared to pure GCE. The slight sluggish behavior experienced at the poly(CoTABImPc) electrode may be accounted for the lesser conductivity and thick film of Pc on the surface which slightly

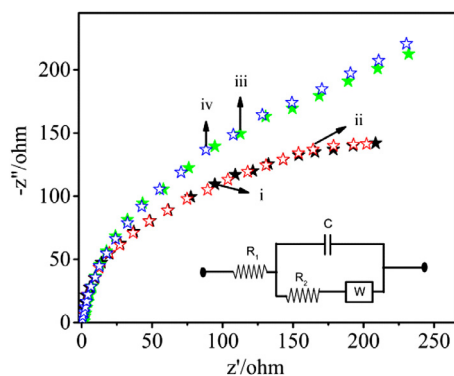


Fig. 3. Nyquist plot of 1 mM $K_4[Fe(CN)_6]$ at (i) bare GCE and (iii) GCE/poly(CoTABImPc) and the theoretical fit for (ii) bare GCE and (iv) GCE/poly(CoTABImPc) in 0.1 M PBS pH 7.0. Inset: Equivalence electrical circuit used to fit the EIS data.

blocks the facile transfer of electrons at the boundary of electrode and electrolyte.

3.9. Impedance spectroscopy

Electrochemical impedance spectroscopy (EIS) is helpful to examine the interfacial charge transfer and charge storage process of the polymeric electrode. Further EIS demonstrates the advantage of separating interfacial processes at different frequency domains. EIS also provides input about the mechanism of reaction arises at the electrode and electrolyte system. EIS was measured in PBS pH 7.0 containing 1 mM $K_4[Fe(CN)_6]$ in the 0.001 Hz to 10,000 Hz frequency range with 5.0 mV amplitude. The Nyquist plot at virgin GCE and poly(CoTABImPc) are placed in Fig. 3. The Randel's equivalent circuit was applied to theoretically fit the Nyquist plot by using the model $R_1(C(R_2W))$ as shown in the inset of Fig. 3, where R_1 , R_2 , C and W symbolize the resistance of solution, charge transfer resistance, capacitance and the complex Warburg impedance, respectively. The semicircle diameter in the Nyquist plot represents the charge transfer resistance. As shown in Fig. 3, GCE/poly(CoTABImPc) displayed larger semicircle diameter than GCE indicating the hindrance of electron transfer from $[Fe(CN)_6]^{3-/4-}$ to electrode owing to the poor conductivity of Pc material. Change in the R_{ct} value of poly(CoTABImPc) compared to the unmodified electrode reveals the modification of poly(CoTABImPc) on the electrode surface. Table S1 summarizes the equivalent electrical circuit parameters evaluated by fitting the impedance spectra.

3.10. Detection of Hg(II)

The GCE/poly(CoTABImPc) electrode was evaluated for the detection of highly toxic Hg(II) by CV in 0.1 M PBS (pH = 7). When 40 nM Hg(II) was added into PBS, a peak appeared at 0.18 V on the GCE/poly(CoTABImPc), which is responsible for the detection of Hg(II), but the bare GCE did not show an appreciable peak for the Hg(II) addition (Fig.S11). The CV revealed that the electrocatalytic current for Hg(II) detection at GCE/poly(CoTABImPc) was much larger with lesser overpotential compared to GCE. The enhanced peak current response and decreased in the overpotential established that the poly(CoTABImPc) film acts as an effective catalyst to activate the detection of analyte.

The augmented electrochemical signal for Hg(II) detection at polymeric film electrode, motivated the concentration-dependent studies at the proposed GCE/poly(CoTABImPc) electrode. Fig. 4a illustrates the CV behavior towards different concentrations of 10 to 300 nM Hg(II) at GCE/poly(CoTABImPc) electrode. The CVs demon-

Table 1

Intrinsic electrochemical parameters for the Hg(II) detection at GCE/poly(CoTABImPc).

Tafel slope	113 mV/dec
Exchange current density	$7.41 \times 10^{-5} \text{ A cm}^{-2}$
Diffusion coefficient	$(2.20 \pm 0.2) \times 10^{-4} \text{ cm}^2 \text{ s}^{-1}$

strated a well-defined and sharp peak for the detection of Hg(II) at 0.18 V and successive increase in response was noticed for enhancement in the Hg(II) concentration. The plot of peak current (i_p) versus the Hg(II) concentration displayed a linear characteristic in the 10–300 nM concentration range (Fig. 4b). The linear equation for the straight-line relationship is; $i_p/\mu\text{A} = 1.2769 + 0.0853 C$ (nM), with the correlation coefficient (R^2) of 0.9979. The sensitivity of the GCE/poly(CoTABImPc) was calculated based on the slope of the calibration plot and the sensitivity was $1.2178 \mu\text{A nM}^{-1} \text{ cm}^{-2}$ with 10 nM as the lowest quantifiable concentration. The experimental limit of detection (LOD) was 4 nM by the 3σ method. The value of LOD for Hg(II) at GCE/poly(CoTABImPc) is much smaller than the reported values in the literature [37–43].

The sensitivity, concentration range and LOD of the fabricated poly(CoTABImPc) electrode are correlated with various modified electrodes in literature for Hg(II) detection and are summarized in Table S2. The LOD offered at GCE/poly(CoTABImPc) is much lower than other electrodes.

The mechanism of Hg(II) detection involves the adsorption of Hg(II) onto the surface of GCE/poly(CoTABImPc) and the presence of benzimidazole and amide groups in the Pc may enhance the adsorption capacity for Hg(II).

3.11. Scan rate studies

The scan rate dependence of the Hg(II) redox reaction at GCE/poly(CoTABImPc) was monitored by CV. The CV curves for 60 nM Hg(II) at various scan rates (10–80 mVs^{-1}) in PBS at GCE/Poly(CoTABImPc) are shown in Fig. 5. The i_p for Hg(II) detection increased with the scan rate ν . Inset of Fig. 5 established that i_p of Hg(II) increased linearly with the square root of the ν from 10 to 80 mVs^{-1} and the linear regression equation for the straight-line characteristics was $i_p/(\mu\text{A}) = 4.5934 ((\text{mVs}^{-1})^{1/2}) + 0.9294x$ with R^2 as 0.9983. The linear variation in i_p with the ν concludes that the Hg(II) detection at the poly(CoTABImPc) electrode is driven by the diffusion process.

The diffusion coefficient, D for the Hg(II) detection at poly(CoTABImPc) is calculated by the Eq. (1),

$$i_p^0 = 0.4463 n FAC (nF\nu D/RT)^{1/2} \quad (1)$$

where n is the total number of electrons transferred in the overall Hg(II) detection reaction ($n = 2$), A is the GCE surface area (0.0701 cm^2), F is the Faraday constant ($96,485.332 \text{ C mol}^{-1}$), C is the bulk Hg(II) concentration (60 nM) in mol cm^{-3} , ν is the scan rate in mVs^{-1} , R is the gas constant ($8.314 \text{ J K}^{-1} \text{ mol}^{-1}$), T is the temperature in K.

The D value was found to be $2.202 \times 10^{-4} \text{ cm}^2\text{s}^{-1}$ for Hg(II) detection at GCE/poly(CoTABImPc) (Table 1) which is comparable with the reported electrodes for Hg(II) [44, 45]. The kinetics of mercury nucleation from Hg_2^{2+} and Hg^{2+} solutions on vitreous carbon electrodes showed D value of ($1.4 \times 10^{-5} \text{ cm}^2\text{s}^{-1}$) [44] and D value for cathodic and anodic deposition of mercury and silver at boron-doped diamond electrodes is ($\sim 10^{-5} \text{ cm}^2\text{s}^{-1}$) [45]. This concludes that GCE/poly(CoTABImPc) has shown a superior D value for Hg(II) compared to other electrodes in the literature. The D value provides an understanding of the ability of Hg(II) to diffuse through a unit area in 1 s in the applied potential gradient of one

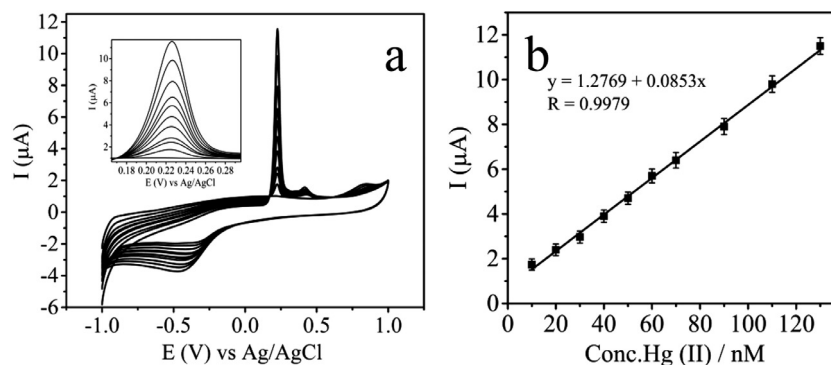


Fig. 4. (a) CV response for Hg(II) in 10 to 300 nM range at GCE/poly(CoTABImPc) in 0.1 M PBS pH 7.0. Inset; zoomed portion of the CV. (b) calibration plot of the peak current versus Hg(II) concentration.

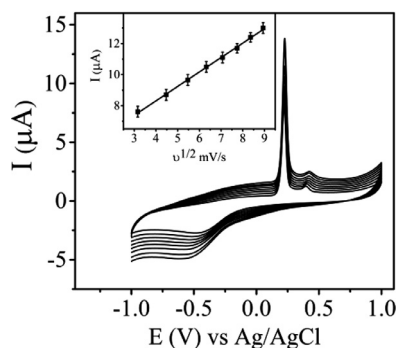


Fig. 5. CVs for 60 nM Hg(II) at GCE/poly(CoTABImPc) in 0.1 M PBS pH 7.0 with different scan rates. Inset: plot for i_p versus square root of scan rate.

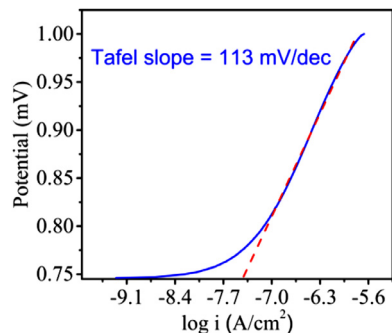


Fig. 6. Tafel plot for the Hg(II) detection at GCE/poly(CoTABImPc).

unit. The D value suggests a facile diffusion of the Hg(II) through the electrolyte to electrode interface.

3.12. Tafel slope

The reaction kinetics and mechanism of Hg(II) detection at GCE/poly(CoTABImPc) can be studied by using Tafel plot, and the slope value in Tafel plot is used to compare the catalytic activities of different electrocatalysts. The Tafel slope value measures the sensitivity of response to an analyte at an appropriate voltage and also explores the rate-determining step for understanding the kinetics of the reaction. The $\log I$ vs. E (V) (Tafel map) is a linear plot with $1/b$ slope. Tafel plot in Fig. 6 follows the typical Tafel performance. The Tafel slope is obtained as 113 mV dec^{-1} for Hg(II) detection at the polymeric electrode. The exchange current density for the rate of the reaction was found to be $7.41 \times 10^{-5} \text{ A cm}^{-2}$ which infers that the intrinsic Hg(II) detection kinetics is aided by the polymerized electrode for the Hg(II) detection at

GCE/poly(CoTABImPc). The Tafel slope value and scan rate studies for Hg(II) detection at GCE/poly(CoTABImPc) show an electrochemically irreversible reaction for the detection of Hg(II). Obtained intrinsic values for the detection of Hg(II) at GCE/poly(CoTABImPc) are shown in Table 1.

3.13. Differential pulse voltammetry

The electrochemical response of the GCE/poly(CoTABImPc) electrode towards Hg(II) detection was also investigated by DPV in PBS (pH 7.0), Fig. 7.

Different concentrations of Hg(II) were added and peak response was monitored under the optimized working conditions. As in Fig. 7a, the GCE/poly(CoTABImPc) demonstrated a gradual increase in peak current with the enhancement of Hg(II) concentration. The relationship between Hg(II) concentration and peak current showed linear range in 10 to 500 nM with straight-line equation $i/\mu\text{A} = 2.6690 + 0.0983 C$ (nM) and a good linear correlation of $R^2 = 0.9961$ with sensitivity as $1.4024 \mu\text{A nM}^{-1} \text{ cm}^{-2}$. Further, the LOD was calculated as 3.8 nM based on the 3σ method. The LOD of this fabricated sensor is lower than that of the reported LOD for electrochemical detection of Hg(II) (Table 2) [37–43].

Fig. 7 confirms that the polymeric Pc exhibits an excellent activity for Hg(II) detection with increased response and sensitivity at GCE/poly(CoTABImPc) interface due to the presence of polymeric phthalocyanine which has an effective interaction or complexing ability with Hg(II).

3.14. Amperometric detection of Hg(II)

The electroanalytical performance of the GCE/poly(CoTABImPc) electrode towards Hg(II) detection was assessed using amperometry. The $i-t$ curve for Hg(II) detection was monitored using PBS pH 7.0 at a fixed potential of 0.18 V and purging the N_2 with constant stirring, Fig. 8. The gradual increase in Hg(II) concentration displayed a proportional current increase and the current response was almost five times higher than the CV and DPV methods indicating the superiority of the amperometric method over CV and DPV methods.

Amperometric response for Hg(II) detection on GCE/poly(CoTABImPc) was quick, and further, the stabilization of the current response takes less than 2–3 s following the subsequent Hg(II) addition. Quick response and faster stabilization time for Hg(II) by the sensor are very important parameters in the fabrication and development of sensor technology. The developed amperometric sensor showed a linear response in 10 to 400 nM range and the linear behavior satisfies the straight-line equation $i/\mu\text{A} = 2.0116 + 0.2621 C$ (nM) with the R^2 , 0.9988 and sensitivity of $3.7389 \mu\text{A nM}^{-1} \text{ cm}^{-2}$. The LOD of Hg(II) was 3 nM

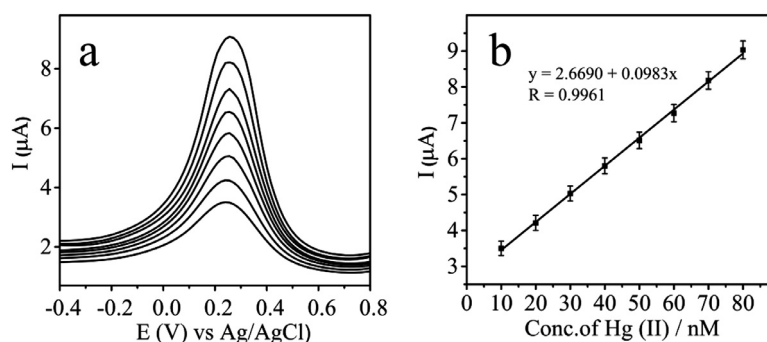


Fig. 7. (a) DPV response of the GCE/poly(CoTABImPc) electrode for the detection of Hg(II) over a concentration range of 10 nM to 500 nM in 0.1 M PBS pH 7.0. (b) calibration plot of the peak current versus Hg(II) concentration.

Table 2

The analytical data of the proposed voltammetric, differential pulse voltammetric and amperometric sensor.

Modifier	Method	Linear Range (nM)	Sensitivity $\mu\text{A nM}^{-1} \text{cm}^{-2}$	LOD (nM)
GCE/poly(CoTABImPc)	CV	10–300	1.2178	4
	DPV	10–500	1.4024	3.8
	CA	10–400	3.7389	3

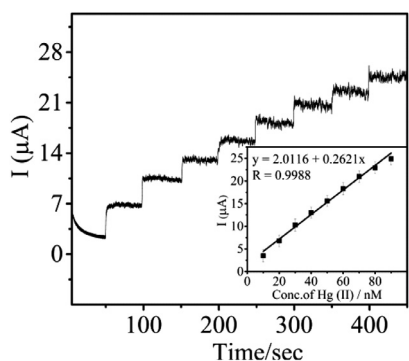


Fig. 8. Amperometric *i-t* curve for Hg(II) of different concentration at GCE/poly(CoTABImPc) in 0.1 M PBS pH 7.0, applied potential 0.18 V. Inset: Plot for current response versus Hg(II) concentration.

by the 3σ method. The fabricated GCE/poly(CoTABImPc) sensor is capable to detect the Hg(II) at lesser concentration levels than the allowed maximum concentration prescribed by the WHO. The analytical data obtained by voltammetric, differential pulse voltammetric and amperometric techniques for the detection of Hg(II) at GCE/poly(CoTABImPc) are tabulated in Table 2.

3.15. Interference, stability and reproducibility of the sensor

The influence of interferences during the Hg(II) detection at GCE/poly(CoTABImPc) was evaluated using various metal ions. The selectivity of the designed GCE/poly(CoTABImPc) was assessed by introducing 5 μM of different metal ions like Pb(II), Cd(II), Zn(II), KCl and 10 nM of Hg(II) in 0.1 M PB solution of pH(7.0), Fig 9. The current response curve (Fig. 9) exhibited a prominent response for Hg(II), whereas even 5000 times larger concentration of other interfering metal ions like Pb(II), Cd(II), Zn(II), and K(I) did not show significant current at designed GCE/poly(CoTABImPc) electrode. Compared to various interferences, the response for Hg(II) on the GCE/poly(CoTABImPc) was much higher representing that the developed electrode selectively responds for Hg(II) even in the presence of higher concentration of interferences (Fig. 9). This shows that the proposed sensor has an excellent anti-interference capability, superior selectivity and recognition capacity for the Hg(II) detection.

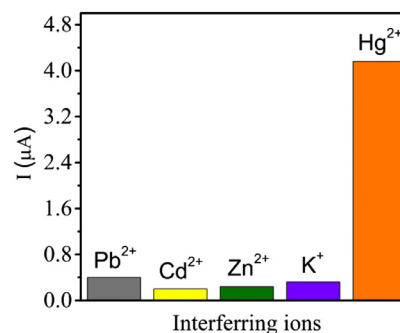


Fig. 9. Selective response for Hg(II) (10 nM) in presence of different heavy metal interfering species like 5 μM Pb(II), Cd(II), Zn(II), and K(I) at the GCE/poly(CoTABImPc) in 0.1 M (pH 7.0) PBS.

The repeatability of the GCE/poly(CoTABImPc) sensor was investigated using the same electrode for 10 successive measurements. This yielded a relative standard deviation (RSD) of 3.31% for 60 nM Hg(II). Furthermore, the electrode-to-electrode reproducibility was measured using 5 modified electrodes, which were fabricated utilizing the same fabrication procedure and it displayed an RSD value of 2.9% for the detection of 60 nM Hg(II).

3.16. Real sample analysis using GCE/poly(CoTABImPc)

The developed GCE/poly(CoTABImPc) sensor was tested for the Hg(II) determination in real samples. Water samples from industrial effluents, pond and river were collected, filtered and used for the Hg(II) analysis at GCE/poly(CoTABImPc) and no response was noticed in the *i-t* curve indicating that either Hg(II) is absent in water samples or it may contain Hg(II) lesser than the applicable range of the GCE/poly(CoTABImPc) sensor. Standard addition method was utilized to study the matrix effect by monitoring the recovery values. A known quantity of Hg(II) was added to the water sample and then *i-t* curve was recorded to find the recovery value. The results are summarized in Table 3 and the recovery of Hg(II) ranged between 98.3 and 102.6% in water samples. Moreover, the RSD (%) values are in between 1.7 and 2.7% demonstrating that the GCE/poly(CoTABImPc) could be practically applied for the Hg(II) determination in real samples.

Table 3
Practical application data obtained for the analysis of different water samples and fish sample.

Sample	Hg(II) found	Spiked (nM L ⁻¹)	Detected (nM L ⁻¹)	Recovery (%)	RSD (%) (n = 3)
River water	-	30	31	103.3	(±2.5)
		100	102	102	(±2.3)
		300	305	101.6	(±1.9)
Industrial effluent water	-	30	31.3	104.3	(±2.8)
		100	104	104	(±2.1)
		300	309	103	(±2.0)
Tap water	-	30	30.7	102.3	(±2.4)
		100	101.5	101.5	(±2.0)
		300	306	102	(±1.6)
Drinking water	-	30	30.2	100.6	(±2.2)
		100	101.6	101.6	(±2.1)
		300	302.5	100.8	(±1.7)
5 g Fish	-	30	30.8	102.6	(±2.8)
		100	100.9	100.9	(±2.6)
		300	304.3	101.4	(±2.3)

RSD-Relative standard deviation for n = 3 measurements.

Further, to apply the polymerized sensor for practical applications, it was also tested for the Hg(II) determination in (angler) fish. The fish sample was purchased from a market in Ballari which was bought from the coastal part of Karnataka, India. 5 g angler fish sample was digested with 20.0 mL concentrated nitric acid at 120 °C for 2 h and then cooled sample was digested in the microwave system for complete digestion. After cooling, the solution was heated at 120 °C to remove the acid. The residue was diluted by PB saline (pH 7.0) to 10 mL and mixed uniformly [46]. Mercury content in the angler fish sample was tested by amperometry and the sample did not yield a significant response inferring that the fish sample contains either no or less Hg(II) than the detectable range of the GCE/poly(CoTABImPc) sensor. The recovery study for angler fish sample was performed and the values are listed in Table 3. The Hg(II) recovery in the fish sample was from 101 to 103% with the relative error below 3%. The results in Table 3 are within an acceptable range and these results reveal that developed GCE/poly(CoTABImPc) sensor acts as an efficient, convenient and consistent platform for monitoring Hg(II) content in real samples.

4. Conclusion

This work presents the fabrication of a phthalocyanine based sensor for the detection of highly toxic Hg(II) heavy metal. Firstly, a novel benzimidazole Pc was synthesized and electropolymerized on the electrode surface. The spectroscopic techniques successfully employed to find the structure and purity of the CoTABImPc. The GCE/poly(CoTABImPc) sensor was applied as an efficient and reliable sensor for the Hg(II) detection at nanomolar concentration. The proposed GCE/poly(CoTABImPc) sensor exhibited superior performance concerning broad linear range, low LOD, good sensitivity. With all these advantages, GCE/poly(CoTABImPc) acts as an efficient electrocatalyst for electrochemical sensing applications.

Declaration of Competing Interest

There are no conflicts of declare.

Credit authorship contribution statement

Manjunatha Palanna: Conceptualization, Writing - original draft, Writing - review & editing. **Shambhulinga Aralekallu:** Validation, Visualization. **CP Keshavananda Prabhu:** Data curation, Formal analysis. **Veeresh A Sajjan:** Resources, Software, Investigation. **Mounesh:** Methodology, Investigation. **Lokesh Koodlur Sanegowda:** Funding acquisition, Project administration, Supervision.

Acknowledgments

Authors acknowledge the financial support from DST-SERB, Govt. of India (No. SERB/F/9388/2016-17), CSIR grant No. 01(2915)/17/EMR-II, DST-FIST support SR/FST/CSI-274/2016 and VGST K-FIST support (GRD No. 555). Manjunatha P acknowledges VSK University, Ballari for the SC/ST fellowship.

Supplementary materials

Supplementary material associated with this article can be found, in the online version, at doi:10.1016/j.electacta.2020.137519.

References

- [1] M.A. Deshmukh, M.D. Shirsat, A. Ramanaviciene, A. Ramanavicius, Composites based on conducting polymers and carbon nanomaterials for heavy metal ion sensing (review), *Crit. Rev. Anal. Chem.* 48 (2018) 293–304, doi:10.1080/10408347.2017.1422966.
- [2] O.S. Akintola, T.A. Saleh, M.M. Khaled, O.C.S. Al Hamouz, Removal of mercury (II) via a novel series of cross-linked polydithiocarbamates, *J. Taiwan Inst. Chem. Eng.* 60 (2016) 602–616, doi:10.1016/j.jtice.2015.10.039.
- [3] K.M. Rice, E.M. Walker, M. Wu, C. Gillette, E.R. Blough, Environmental mercury and its toxic effects, *J. Prev. Med. Public Health* 47 (2014) 74–83, doi:10.3961/jpmph.2014.47.2.74.
- [4] S. Palanisamy, K. Thangavelu, S.M. Chen, V. Velusamy, M.H. Chang, T.W. Chen, F.M.A. Al-Hemaid, M.A. Ali, S.K. Ramaraj, Synthesis and characterization of polypyrrole decorated graphene/ β -cyclodextrin composite for low level electrochemical detection of mercury (II) in water, *Sens. Actuators B Chem.* 243 (2017) 888–894, doi:10.1016/j.snb.2016.12.068.
- [5] Y. Bhattacharjee, A. Chakraborty, Label-free cysteamine-capped silver nanoparticle-based colorimetric assay for Hg(II) detection in water with subnanomolar exactitude, *ACS Sustain. Chem. Eng.* 2 (2014) 2149–2154, doi:10.1021/sc500339n.
- [6] R.S. Hughner, J.K. Maher, N.M. Childs, Review of food policy and consumer issues of mercury in fish, *J. Am. Coll. Nutr.* 27 (2008) 185–194, doi:10.1080/07315724.2008.10719690.
- [7] I. Serafimovski, I. Karadjova, T. Stafilov, J. Cvetković, Determination of inorganic and methylmercury in fish by cold vapor atomic absorption spectrometry and inductively coupled plasma atomic emission spectrometry, *Microchem. J.* 89 (2008) 42–47, doi:10.1016/j.microc.2007.11.003.
- [8] T. Swanston, T. Varney, I. Coulthard, G.N. George, I.J. Pickering, R. Murphy, D.M.L. Cooper, Synchrotron X-ray fluorescence imaging evidence of biogenic mercury identified in a burial in colonial antigua, *J. Archaeol. Sci.* 58 (2015) 26–30, doi:10.1016/j.jas.2015.03.006.
- [9] C.H. Yao, S.J. Jiang, A.C. Sahayam, Y.L. Huang, Speciation of mercury in fish oils using liquid chromatography inductively coupled plasma mass spectrometry, *Microchem. J.* 133 (2017) 556–560, doi:10.1016/j.microc.2017.04.034.
- [10] X.P. Yan, X.B. Yin, D.Q. Jiang, X.W. He, Speciation of mercury by hydrostatically modified electroosmotic flow capillary electrophoresis coupled with volatile species generation atomic fluorescence spectrometry, *Anal. Chem.* 75 (2003) 1726–1732, doi:10.1021/ac026272x.
- [11] Q. Jiang, H. Wang, X. Wei, Y. Wu, W. Gu, L. Hu, C. Zhu, Efficient BiVO₄ photoanode decorated with Ti₃C₂TX MXene for enhanced photoelectrochemical sensing of Hg(II) ion, *Anal. Chim. Acta* 1119 (2020) 11–17, doi:10.1016/j.aca.2020.04.049.

- [12] J.C.C. Yu, E.P.C. Lai, S. Sadeghi, Surface plasmon resonance sensor for Hg(II) detection by binding interactions with polypyrrole and 2-mercaptobenzothiazole, *Sens. Actuators B Chem.* 101 (2004) 236–241, doi:10.1016/j.snb.2004.03.007.
- [13] X. Ding, L. Kong, J. Wang, F. Fang, D. Li, J. Liu, Highly sensitive SERS detection of Hg²⁺ ions in aqueous media using gold nanoparticles/graphene heterojunctions, *ACS Appl. Mater. Interfaces* 5 (2013) 7072–7078, doi:10.1021/am401373e.
- [14] G. Wen, W. Zhao, X. Chen, J. Liu, Y. Wang, Y. Zhang, Z. Huang, Y. Wu, N-doped reduced graphene oxide /MnO₂ nanocomposite for electrochemical detection of Hg²⁺ by square wave stripping voltammetry, *Electrochim. Acta* (2018), doi:10.1016/j.electacta.2018.08.121.
- [15] J. Ke, X. Li, Q. Zhao, Y. Hou, J. Chen, Ultrasensitive quantum dot fluorescence quenching assay for selective detection of mercury ions in drinking water, *Sci. Rep.* 4 (2014) 4–9, doi:10.1038/srep05624.
- [16] K. Chen, S. She, J. Zhang, A. Bayaguud, Y. Wei, Label-free colorimetric detection of mercury via Hg²⁺ ions-accelerated structural transformation of nanoscale metal-oxo clusters, *Sci. Rep.* 5 (2015) 1–9, doi:10.1038/srep16316.
- [17] D.D. Eley, Phthalocyanine as semiconductor, *Nature* 162 (1948) 819.
- [18] L.S. Koodlur, Layer-by-layer self assembly of a water-soluble phthalocyanine on gold. Application to the electrochemical determination of hydrogen peroxide, *Bioelectrochemistry* 91 (2013) 21–27, doi:10.1016/j.bioelechem.2012.12.001.
- [19] V.A. Sajjan, S. Aralekallu, M. Nemakal, M. Palanna, C.P.K. Prabhu, L.K. Sannegowda, Nanomolar detection of lead using electrochemical methods based on a novel phthalocyanine, *Inorganica Chim. Acta* 506 (2020) 119564, doi:10.1016/j.ica.2020.119564.
- [20] I. Mohammed, M. Nemakal, S. Aralekallu, V.A. Sajjan, T.R. Divakara, M. Palanna, C.P. Keshavananda Prabhu, L.K. Sannegowda, Phthalocyanine sheet polymer based amperometric sensor for the selective detection of 2,4-dichlorophenol, *J. Electroanal. Chem.* 871 (2020) 114292, doi:10.1016/j.jelechem.2020.114292.
- [21] B.O. Agboola, K.I. Ozoemena, Synergistic enhancement of supercapacitance upon integration of nickel (II) octa [(3,5-bis(carboxylate)-phenoxy) phthalocyanine with SWCNT-phenylamine, *J. Power Sources* 195 (2010) 3841–3848, doi:10.1016/j.jpowsour.2009.12.095.
- [22] Y. Bian, L. Su, Z. Yu, Z. Lv, H. Chen, Y. Zhou, C. Meng, H. Du, M. Cai, H. Cao, M.C. Lin, Graphite/copper phthalocyanine composite cathode for overcharge protection and gas evolution suppression in aluminum-ion batteries at room temperature, *Electrochim. Acta* 332 (2020), doi:10.1016/j.electacta.2019.135188.
- [23] R.R. Mather, The Effect of crystal properties on the manufacture and application performance of copper phthalocyanine pigments, *J. Porphyr. Phthalocyanines* 3 (1999) 643–646, doi:10.1002/(sici)1099-1409(199908/10)3:6/7(643::aid-jpp187)3.0.co;2-v.
- [24] S. Aralekallu, V.A. Sajjan, M. Palanna, K. Prabhu C P, M. Hojamberdiev, L.K. Sannegowda, Ni foam-supported azo linkage cobalt phthalocyanine as an efficient electrocatalyst for oxygen evolution reaction, *J. Power Sources* 449 (2020) 227516, doi:10.1016/j.jpowsour.2019.227516.
- [25] R. Praats, M. Käärik, A. Kikas, V. Kisan, J. Aruväli, P. Paiste, M. Merisalu, J. Leis, V. Sammelselg, J.H. Zagal, S. Holdcroft, N. Nakashima, K. Tammeveski, Electro-catalytic oxygen reduction reaction on iron phthalocyanine-modified carbide-derived carbon/carbon nanotube composite electrocatalysts, *Electrochim. Acta* 334 (2020), doi:10.1016/j.electacta.2019.135575.
- [26] M. Shumba, T. Nyokong, Development of nanocomposites of phosphorus-nitrogen co-doped graphene oxide nanosheets and nanosized cobalt phthalocyanines for electrocatalysis, *Electrochim. Acta* 213 (2016) 529–539, doi:10.1016/j.electacta.2016.07.079.
- [27] C. Gutiérrez-Ceron, R. Oñate, J.H. Zagal, A. Pizarro, J.F. Silva, C. Castro-Castillo, M.C. Rezende, M. Flores, D. Cortés-Arriagada, A. Toro-Labbé, L.M. Campos, L. Venkataraman, I. Ponce, Molecular conductance versus inductive effects of axial ligands on the electrocatalytic activity of self-assembled iron phthalocyanines: the oxygen reduction reaction, *Electrochim. Acta* 327 (2019) 134996, doi:10.1016/j.electacta.2019.134996.
- [28] C.P. Keshavananda Prabhu, M. Nemakal, S. Aralekallu, I. Mohammed, M. Palanna, V.A. Sajjan, D. Akshitha, L.K. Sannegowda, A comparative study of carboxylic acid and benzimidazole phthalocyanines and their surface modification for dopamine sensing, *J. Electroanal. Chem.* 847 (2019) 113262, doi:10.1016/j.jelechem.2019.113262.
- [29] M. Palanna, I. Mohammed, S. Aralekallu, M. Nemakal, L.K. Sannegowda, Simultaneous detection of paracetamol and 4-aminophenol at nanomolar levels using biocompatible cysteine-substituted phthalocyanine, *New J. Chem* 44 (2020) 1294–1306, doi:10.1039/c9nj05252f.
- [30] S. Aralekallu, I. Mohammed, N. Manjunatha, M. Palanna, Dhanjai, L.K. Sannegowda, Synthesis of novel azo group substituted polymeric phthalocyanine for amperometric sensing of nitrite, *Sens. Actuators B Chem.* (2019) 417–425, doi:10.1016/j.snb.2018.11.093.
- [31] H. Zhong, R. Tian, X. Gong, D. Li, P. Tang, N. Alonso-Vante, Y. Feng, Advanced bifunctional electrocatalyst generated through cobalt phthalocyanine tetrasulfonate intercalated Ni₂Fe-layered double hydroxides for a laminar flow unutilized regenerative micro-cell, *J. Power Sources* 361 (2017) 21–30, doi:10.1016/j.jpowsour.2017.06.057.
- [32] Z. Zhang, J. Xiao, X.J. Chen, S. Yu, L. Yu, R. Si, Y. Wang, S. Wang, X. Meng, Y. Wang, Z.Q. Tian, D. Deng, Reaction mechanisms of well-defined metal-N₄ sites in electrocatalytic CO₂ reduction, *Angew. Chem. – Int. Ed.* 57 (2018) 16339–16342, doi:10.1002/anie.201808593.
- [33] I. Mohammed, M. Nemakal, V.A. Sajjan, D.B. Puttappashetty, L.K. Sannegowda, Electropolymerized film of cobalt tetrabenzimidazole phthalocyanine for the amperometric detection of H₂O₂, *J. Electroanal. Chem.* 826 (2018) 96–103, doi:10.1016/j.jelechem.2018.08.029.
- [34] N. Manjunatha, M. Imadadulla, K.S. Lokesh, K.R. Venugopala Reddy, Synthesis and electropolymerization of tetra-[β-(2-benzimidazole)] and tetra-[β-(2-(1-(4-aminophenyl)benzimidazole))] embedded cobalt phthalocyanine and their supercapacitance behaviour, *Dye. Pigment* 153 (2018) 213–224, doi:10.1016/j.dyepig.2018.01.042.
- [35] O.O. Ajani, O.O. Tolu-Bolaji, S.J. Olorunshola, Y. Zhao, D.V. Aderohunmu, Structure-based design of functionalized 2-substituted and 1,2-disubstituted benzimidazole derivatives and their in vitro antibacterial efficacy, *J. Adv. Res.* 8 (2017) 703–712, doi:10.1016/j.jare.2017.09.003.
- [36] E. Valeur, M. Bradley, Amide bond formation: beyond the myth of coupling reagents, *Chem. Soc. Rev.* 38 (2009) 606–631, doi:10.1039/b701677h.
- [37] J. Lu, X. Zhang, X. Zhang, N. Liu, H. Li, Z. Yu, X. Yan, Electrochemical sensor for mercuric chloride based on graphene-MnO₂ composite as recognition element, *Electrochim. Acta* 174 (2015) 221–229, doi:10.1016/j.electacta.2015.05.181.
- [38] S. Xiong, B. Yang, D. Cai, G. Qiu, Z. Wu, Individual and simultaneous stripping voltammetric and mutual interference analysis of Cd²⁺, Pb²⁺ and Hg²⁺ with reduced graphene oxide-Fe₃O₄ nanocomposites, *Electrochim. Acta* 185 (2015) 52–61, doi:10.1016/j.electacta.2015.10.114.
- [39] H. Xing, J. Xu, X. Zhu, X. Duan, L. Lu, W. Wang, Y. Zhang, T. Yang, Highly sensitive simultaneous determination of cadmium (II), lead (II), copper (II), and mercury (II) ions on N-doped graphene modified electrode, *J. Electroanal. Chem.* 760 (2016) 52–58, doi:10.1016/j.jelechem.2015.11.043.
- [40] X. Xu, G. Duan, Y. Li, G. Liu, J. Wang, H. Zhang, Z. Dai, W. Cai, Fabrication of gold nanoparticles by laser ablation in liquid and their application for simultaneous electrochemical detection of Cd²⁺, Pb²⁺, Cu²⁺, Hg²⁺, *ACS Appl. Mater. Interfaces* 6 (2014) 65–71, doi:10.1021/am404816e.
- [41] S. Muralikrishna, K. Sureshkumar, T.S. Varley, D.H. Nagaraju, T. Ramakrishnappa, In situ reduction and functionalization of graphene oxide with L-cysteine for simultaneous electrochemical determination of cadmium(II), lead(II), copper(II), and mercury(II) ions, *Anal. Methods* 6 (2014) 8698–8705, doi:10.1039/c4ay01945h.
- [42] I. Cesarino, G. Marino, J.do R. Matos, É.T.G. Cavalheiro, Evaluation of a carbon paste electrode modified with organofunctionalised SBA-15 nanostructured silica in the simultaneous determination of divalent lead, copper and mercury ions, *Talanta* 75 (2008) 15–21, doi:10.1016/j.talanta.2007.06.032.
- [43] M.A. Deshmukh, R. Celiesiute, A. Ramanaviciene, M.D. Shirsat, A. Ramanavicius, EDTA_PANI/SWCNTs nanocomposite modified electrode for electrochemical determination of copper (II), lead (II) and mercury (II) ions, *Electrochim. Acta* 259 (2018) 930–938, doi:10.1016/j.electacta.2017.10.131.
- [44] N. Vinokur, Cathodic and anodic deposition of mercury and silver at boron-doped diamond electrodes, *J. Electrochem. Soc.* 146 (1999) 125, doi:10.1149/1.1391574.
- [45] A. Serruya, J. Mostany, B.R. Scharifker, Kinetics of mercury nucleation from Hg₂²⁺ and Hg²⁺ solutions on vitreous carbon electrodes, *J. Electroanal. Chem.* 464 (1999) 39–47, doi:10.1016/S0022-0728(98)00464-1.
- [46] Q. Zhao, S. Chen, L. Zhang, H. Huang, Y. Zeng, F. Liu, Multiplex sensor for detection of different metal ions based on on-off of fluorescent gold nanoclusters, *Anal. Chim. Acta* 852 (2014) 236–243, doi:10.1016/j.aca.2014.09.029.